A Letters Journal Exploring the Frontiers of Physics

November 2018

EPL, **124** (2018) 40004
doi: 10.1209/0295-5075/124/40004

www.epljournal.org

Inverse stochastic resonance in a system of excitable active rotators with adaptive coupling

Iva Bačić[1], Vladimir Klinshov[2], Vladimir Nekorkin[2], Matjaž Perc[3] and Igor Franović[1(a)]

[1] *Scientific Computing Laboratory, Center for the Study of Complex Systems, Institute of Physics Belgrade, University of Belgrade - Pregrevica 118, 11080 Belgrade, Serbia*
[2] *Institute of Applied Physics of the Russian Academy of Sciences - 46 Ulyanov Street, 603950 Nizhny Novgorod, Russia*
[3] *Faculty of Natural Sciences and Mathematics, University of Maribor - Koroška cesta 160, SI-2000 Maribor, Slovenia*

received 17 September 2018; accepted in final form 8 November 2018
published online 11 December 2018

PACS 05.40.Ca – Noise
PACS 87.19.ln – Oscillations and resonance

Abstract – Inverse stochastic resonance is a phenomenon where an oscillating system influenced by noise exhibits a minimal oscillation frequency at an intermediate noise level. We demonstrate a novel generic scenario for such an effect in a multi-timescale system, considering an example of emergent oscillations in two adaptively coupled active rotators with excitable local dynamics. The impact of plasticity turns out to be twofold. First, at the level of multiscale dynamics, one finds a range of intermediate adaptivity rates that give rise to multistability between the limit cycle attractors and the stable equilibria, a condition necessary for the onset of the effect. Second, applying the fast-slow analysis, we show that the plasticity also plays a facilitatory role on a more subtle level, guiding the fast flow dynamics to parameter domains where the stable equilibria become focuses rather than nodes, which effectively enhances the influence of noise. The described scenario persists for different plasticity rules, underlying its robustness in the light of potential applications to neuroscience and other types of cell dynamics.

Introduction. – Noise in coupled excitable or bistable systems may induce two types of generic effects [1]. On the one hand, it can modify the deterministic behavior by acting non-uniformly on different states of the system, thus amplifying or suppressing some of its features. On the other hand, noise may give rise to completely novel forms of behavior, typically based on crossing the thresholds or separatrices, or involving enhanced stability of deterministically unstable structures. In neuronal systems, the constructive role of noise at different stages of information processing, referred to as "stochastic facilitation" [2,3], mainly comprises resonant phenomena. A classical example is the stochastic resonance [4], which allows for the detection of weak subthreshold periodic signals. A more recent development concerns the effect of inverse stochastic resonance (ISR) [3,5–12], where noise selectively reduces the spiking frequency of neuronal oscillators, converting the tonic firing into intermittent bursting-like activity or a short-lived transient followed by a long period of quiescence. The name of the effect should be taken *cum grano salis*, because in contrast to stochastic resonance, it involves no additional external signal: one rather observes a non-monotonous dependence of the spiking rate on noise variance, whereby the oscillation frequency becomes minimal at a preferred noise level. Such an inhibitory effect of noise has recently been shown for cerebellar Purkinje cells [11], having explicitly demonstrated how the lifetimes of the spiking ("up") and the silent ("down") states [13–15] are affected by the noise variance. ISR has been indicated to play important functional roles in neuronal systems, including the reduction of spiking frequency in the absence of neuromodulators, suppression of pathologically long short-term memories, triggering of on-off tonic spiking activity and even optimization of information transfer along the signal propagation pathways [3,7,9,11].

So far, theoretical studies on ISR have mostly concerned the scenario where a single neuron exhibits bistable deterministic dynamics, featuring coexistence between a limit cycle and a stable equilibrium. Such bistability is

(a) E-mail: franovic@ipb.ac.rs

typical for Type-II neurons below the subcritical Hopf bifurcation, *e.g.*, classical Hodgkin-Huxley and Morris-Lecar models [3,6–8]. There, applying noise induces switching between the metastable states, but at an intermediate noise level, one surprisingly finds a strong asymmetry of the associated switching rates, which makes the periods spent in the vicinity of equilibrium much longer than the periods of spiking activity.

An important open problem concerns conditions giving rise to ISR in coupled excitable systems, where noise influences the emergent oscillations. Here we address in detail this issue, as it may be crucial to understanding the prevalence of the effect in neural networks, whose activity depends on the interplay of excitability, coupling properties and noise. Synaptic dynamics typically involves the plasticity feature, which makes self-organization in neuronal systems a multi-timescale process: the short-term spiking activity unfolds on a quasi-static coupling configuration, while the slow adjustment of coupling weights depends on the time-averaged evolution of units.

Motivated by the findings in neuroscience, we focus on the onset of ISR in a simplified, yet paradigmatic system of two adaptively coupled stochastic active rotators with excitable local dynamics. Active rotators are canonical for Type-I excitability and may be seen as equivalent to the theta-neuron model. Adaptivity is introduced in a way that allows continuous interpolation between a spectrum of plasticity rules, including Hebbian learning and spike-time-dependent plasticity (STDP) [16–18].

We demonstrate a generic scenario for the plasticity-induced ISR, where the system's multiscale structure, defined by the adaptivity rate, plays a crucial role. On a basic level, plasticity gives rise to multistable behavior involving coexisting stationary and oscillatory regimes. An additional subtlety, which we show by the fast-slow analysis, is that the plasticity promotes the resonant effect by guiding the fast flow toward the parameter region where the stable fixed points are focuses rather than nodes.

The paper is organized as follows. In the next section the details of the model and the numerical bifurcation analysis of the deterministic dynamics are presented. The third section contains the results on the ISR effect and the supporting conditions. In the fourth section the fast-slow analysis is applied to explain the mechanism by which plasticity enhances the system's non-linear response to noise. Apart from providing a brief summary, in the last section we also discuss the prevalence of the observed effect.

Model and bifurcation analysis of deterministic dynamics. – Our model involves two stochastic active rotators interacting by adaptive couplings [19–22],

$$\begin{aligned}
\dot{\varphi_1} &= I_0 - \sin\varphi_1 + \kappa_1 \sin(\varphi_2 - \varphi_1) + \sqrt{D}\xi_1(t), \\
\dot{\varphi_2} &= I_0 - \sin\varphi_2 + \kappa_2 \sin(\varphi_1 - \varphi_2) + \sqrt{D}\xi_2(t), \\
\dot{\kappa_1} &= \epsilon(-\kappa_1 + \sin(\varphi_2 - \varphi_1 + \beta)), \\
\dot{\kappa_2} &= \epsilon(-\kappa_2 + \sin(\varphi_1 - \varphi_2 + \beta)),
\end{aligned} \tag{1}$$

where the phases $\{\varphi_1, \varphi_2\} \in S^1$, while the coupling weights $\{\kappa_1, \kappa_2\}$ are real variables.

The excitability parameters I_0, which one may interpret as external bias currents in the context of neuroscience, are assumed to be identical for both units. For such a setup, the deterministic version of (1) possesses a Z_2 symmetry, being invariant to the exchange of units' indices. The uncoupled units undergo a SNIPER bifurcation at $I_0 = 1$, with the values $I_0 < 1\,(I_0 > 1)$ corresponding to the excitable (oscillatory) regime. We consider the case of excitable local dynamics, keeping $I_0 = 0.95$ fixed throughout the paper, such that the oscillations may emerge only due to the coupling terms and/or noise. The scale separation between the fast dynamics of the phases and the slow dynamics of adaptation is adjusted by the parameter $\epsilon \ll 1$. The fast variables are influenced by independent white noise of variance D such that $\xi_i(t)\xi_j(t') = \delta_{ij}\delta(t-t')$ for $i, j \in \{1, 2\}$. Conceptually, adding stochastic input to the fast variables embodies the action of synaptic noise in neuronal systems [23].

The modality of the plasticity rule is specified by the parameter β, whose role may be understood by invoking the qualitative analogy between the adaptation dynamics in classical neuronal systems and the systems of coupled phase oscillators. This issue has first been addressed in [24–26], and a deeper analysis of the correspondence between the phase-dependent plasticity rules and the STDP has been carried out in [19]. In particular, it has been shown that the plasticity dynamics for $\beta = 3\pi/2$, where the stationary weights between the oscillators with smaller/larger phase differences increase/decrease, qualitatively resembles the Hebbian learning rule [25,26]. Nevertheless, when $\beta = \pi$, the coupling weights encode a causal relationship between the spiking of oscillators by changing in the opposite directions, in analogy to an STDP-like plasticity rule. Our interest lies with the β interval interpolating between these two limiting cases.

Using bifurcation analysis of the deterministic dynamics of (1), we first show how the modality of the plasticity rule influences the number of stationary states, and then explain how the onset of oscillations depends on adaptivity rate. The bifurcation diagram in fig. 1 indicates that the number and the stability of fixed points of (1) change with β in such a way that the system may possess two, four or six fixed points. Due to invariance to Z_2 symmetry, one always finds pairs of solutions sharing the same stability features. We consider the plasticity rules described by $\beta \in (3.298, 4.495)$, cf. the shaded region in fig. 1, where the system has two stable fixed points lying off the synchronization manifold $\varphi_1 = \varphi_2$, as well as four unstable fixed points. The bifurcations occurring at the boundaries of the relevant β interval are as follows. At $\beta = 3.298$, the system undergoes a supercritical symmetry-breaking pitchfork bifurcation giving rise to a pair of stable fixed points off the synchronization manifold. For $\beta = 4.495$, this pair of stable fixed points collides with a pair of unstable fixed points off

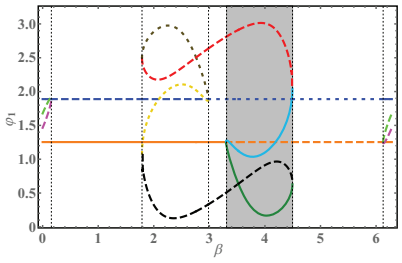

Fig. 1: (Color online) Bifurcation diagram for the fixed points of (1) with $D = 0$ under variation of β. Solid lines refer to stable fixed points, while dashed and dotted lines correspond to saddles of unstable dimension 1 and 2, respectively. Shading indicates the considered range of plasticity rules. The two fixed points independent on β belong to the synchronization manifold. The remaining parameters are $I_0 = 0.95, \epsilon = 0.05$.

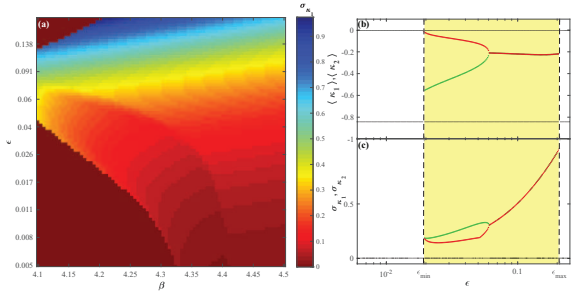

Fig. 2: (Color online) Onset of oscillations in (1) for $D = 0$. (a) Variation σ_{κ_1} of the coupling weight κ_1 in the (β, ϵ)-plane. (b) Mean coupling weights $\langle\kappa_1\rangle(\epsilon)$ and $\langle\kappa_2\rangle(\epsilon)$ for oscillatory (thick lines) and stationary states (thin lines) at $\beta = 4.2$. (c) Variation $\sigma_{\kappa_1}(\epsilon)$ and $\sigma_{\kappa_2}(\epsilon)$, presented as in (b). Shading in (b) and (c) indicates the ϵ interval admitting the stable periodic solutions.

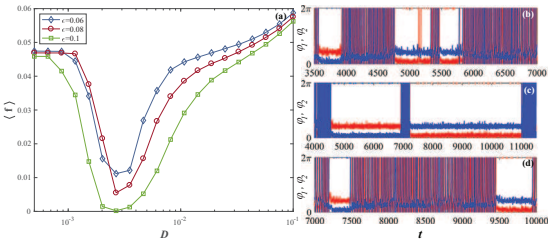

Fig. 3: (Color online) (a) Mean spiking rate $\langle f\rangle$ in terms of D for $\epsilon \in \{0.06, 0.08, 0.1\}$. The curves exhibit a characteristic minimum at an intermediate noise level. (b)–(d) Time traces $\varphi_1(t)$ and $\varphi_2(t)$ for noise levels below, at and above the resonant value. The remaining parameters are $I_0 = 0.95$, $\beta = 4.2, \epsilon = 0.06$.

the synchronization manifold, getting annihilated in two symmetry- related inverse fold bifurcations. Note that the weight levels typical for the two stable stationary states support effective unidirectional interaction, in a sense that one unit exerts a much stronger impact on the dynamics of the other unit than vice versa. When illustrating the effect of ISR, we shall mainly refer to the case $\beta = 4.2$. For this β, the two stable focuses of (1) at $D = 0$ are given by $(\varphi_1, \varphi_2, \kappa_1, \kappa_2) = (1.177, 0.175, 0.032, -0.92)$ and $(\varphi_1, \varphi_2, \kappa_1, \kappa_2) = (0.175, 1.177, -0.92, 0.032)$. Within the considered β interval, the two stable fixed points of the coupled system exhibit excitable behavior, responding to external perturbation by generating either the successive spikes or synchronized spikes [21].

The onset of oscillations for the deterministic version of (1) relies on the interplay between the plasticity rule, controlled by β, and the adaptation rate, characterized by ϵ. In fig. 2(a) are shown the results of parameter sweep indicating the variation of κ_1 variable, $\sigma_{\kappa_1} = \max(\kappa_1(t)) - \min(\kappa_1(t))$, within the (β, ϵ) parameter plane. The sweep indicates the maximal stability region of the two emerging periodic solutions, related by the exchange symmetry of units indices. The data are obtained by numerical continuation starting from a stable periodic solution, such that the final state reached for the given parameter set is used as initial conditions of the system dynamics for incremented parameter values. One observes that for fixed β, there exists an interval of timescale separation ratios $\epsilon \in (\epsilon_{min}, \epsilon_{max})$ admitting oscillations, see fig. 2(b). Within the given ϵ range, the system exhibits multistability where periodic solutions coexist with the two symmetry-related stable stationary states. The lower threshold for oscillations, ϵ_{min}, reduces with β, whereas the upper boundary value, ϵ_{max}, is found to grow as β is enhanced. Note that the waveform of oscillations also changes as ϵ is increased under fixed β. In particular, for smaller ϵ, the waveforms corresponding to the two units are rather different. Nevertheless, around $\epsilon \approx 0.06$ the system undergoes a pitchfork bifurcation of limit cycles, such that the oscillatory solution gains the anti-phase space-time symmetry $\varphi_1(t) = \varphi_2(t + T/2), \kappa_1(t) = \kappa_2(t + T/2)$, where T denotes the oscillation period [21].

Numerical results on ISR. – Inverse stochastic resonance manifests itself as noise-mediated suppression of oscillations, whereby the frequency of noise-perturbed oscillations becomes minimal at a preferred noise level. For system (1), we find such an effect to occur generically for intermediate adaptivity rates, supporting multistability between the stationary and the oscillatory solutions, as described in the previous section. A family of curves describing the dependence of the oscillation frequency on noise variance $\langle f\rangle(D)$ for different ϵ values is shown in fig. 3. All the curves corresponding to $\epsilon \geq \epsilon_{min}(\beta)$ show a characteristic non-monotonous behavior, displaying a minimum at the optimal noise intensity. For weaker noise, the oscillation frequency remains close to the deterministic one, whereas for much stronger noise, the frequency increases above that of unperturbed oscillations. The displayed results are obtained by averaging over an ensemble of 1000 different stochastic realizations, having excluded the transient behavior, and having fixed a single set of initial conditions within the basin of attraction of the limit cycle attractor. Nevertheless, we have verified that the

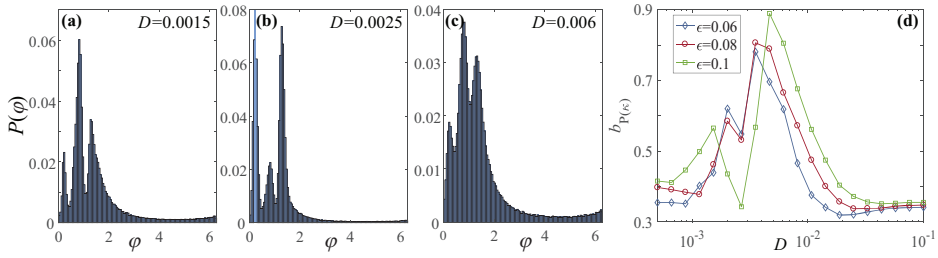

Fig. 4: (Color online) (a)–(c) Stationary distribution $P(\varphi_1)$ for the noise levels below, at and above the resonant value. System parameters are $I_0 = 0.95$, $\beta = 4.2$ and $\epsilon = 0.06$. From the three observable peaks, the middle one, prevalent in (a) and (c), refers to the metastable state associated to the oscillatory mode of (1) for $D = 0$. The two lateral peaks, dominant in (b), correspond to quasi-stationary states derived from the stable equilibria of the deterministic version of (1). (d) Bimodality coefficient for the stationary distribution of κ_1, $b_{P(\kappa_1)}$, as a function of D. The three curves refer to $\epsilon = 0.06$ (diamonds), $\epsilon = 0.08$ (circles) and $\epsilon = 0.1$ (squares).

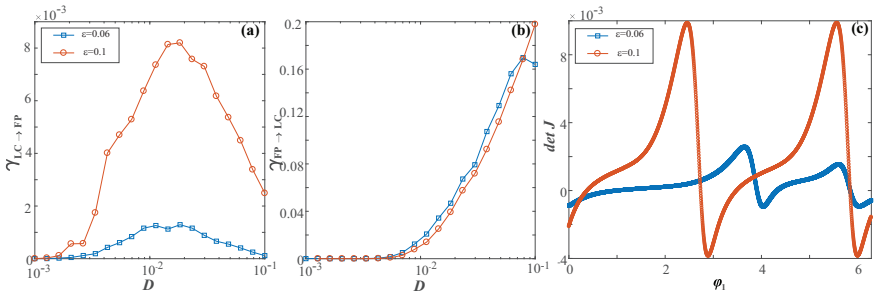

Fig. 5: (Color online) (a) and (b): transition rates from the stability basin of the limit cycle to the fixed point, $\gamma_{LC\to FP}(D)$ and vice versa, $\gamma_{FP\to LC}(D)$, numerically obtained for $\epsilon = 0.06$ (squares) and $\epsilon = 0.1$ (circles). The remaining parameters are $I_0 = 0.95, \beta = 4.2$. (c) Determinant of the Jacobian calculated along the limit cycle orbit as a function of the phase variable. The quantity provides an indication of the sensitivity of certain sections of the orbit to external perturbation. Blue and red colors correspond to $\epsilon = 0.06$ and $\epsilon = 0.1$, respectively.

qualitatively analogous results are obtained if for each realization of stochastic process one selects a set of random initial conditions lying within the stability basin of the periodic solution. The suppression effect of noise depends on the adaptivity rate, and is found to be more pronounced for faster adaptivity. Indeed, for smaller ϵ, $\varphi(t)$ series corresponding to the noise levels around the minimum of $\langle f\rangle(D)$ exhibit bursting-like behavior, whereas for larger ϵ, noise is capable of effectively quenching the oscillations, such that the minimal observed frequency approaches zero.

The core of the described effect concerns switching dynamics between the metastable states associated to coexisting attractors of the deterministic version of system (1). To illustrate this, in fig. 4 we have considered the stationary distributions of one of the phase variables, $P(\varphi)$, for the noise levels below, at and above the minimum of the $\langle f\rangle(D)$, having fixed the remaining parameters to $(\beta, \epsilon) = (4.2, 0.06)$. The distribution $P(\varphi)$ is characterized by two lateral peaks, reflecting the two symmetry-related quasi-stationary states, and the area around the central peak, corresponding to the oscillatory mode. For small noise $D = 0.0015$, see fig. 4(a), and very large noise $D = 0.006$, cf. fig. 4(c), the central peak of $P(\varphi)$ is expectedly prevalent compared to the two lateral peaks. Nevertheless, the switching dynamics for $D = 0.0025$, the noise level about the minimum of $\langle f\rangle(D)$, is fundamentally different, and the corresponding distribution $P(\varphi)$ in fig. 4(b) shows that the system spends much more time in the quasi-stationary states than performing the oscillations. The onset of ISR in the dynamics of fast variables is accompanied by the increased bimodality of the stationary distribution of the couplings, see fig. 4(d).

In order to observe the non-monotonous response of the system's frequency to noise, the geometry of the phase space has to be asymmetrical with respect to the separatrix between the coexisting attractors in such a way that the limit cycle attractor lies much closer to the separatrix than the stationary states. Such structure of phase space gives rise to asymmetry in switching dynamics, whereby at the preferred noise level around the minimum of $\langle f\rangle(D)$, the transition rate from the stability basin of the limit cycle attractor to that of stationary states $\gamma_{LC\to FP}$ becomes much larger than the transition rate in the inverse direction, $\gamma_{FP\to LC}$. Figures 5(a) and (b) corroborate that the dependences $\gamma_{LC\to FP}(D)$ and $\gamma_{FP\to LC}(D)$ are qualitatively distinct: the former displays a maximum at the resonant noise level, whereas the latter just increases monotonously with noise. The fact that ISR is more pronounced for higher adaptivity rates is reflected in that the curve $\gamma_{LC\to FP}(D)$ for $\epsilon = 0.1$ lies substantially above that for $\epsilon = 0.06$, see fig. 5(a).

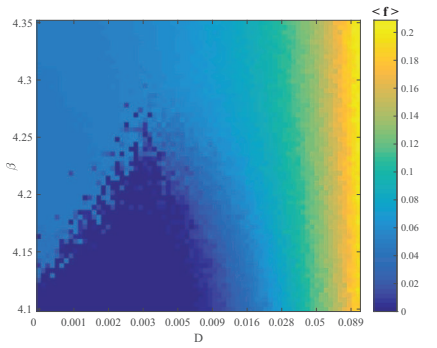

Fig. 6: (Color online) Mean spiking rate $\langle f \rangle$ as a function of β and D for fixed $\epsilon = 0.05$. The results evince the robustness of the ISR effect with respect to different plasticity rules.

To understand why the interplay of adaptivity rate and noise yields a stronger resonant effect for larger ϵ, we have investigated the susceptibility of the limit cycle attractor to external perturbation. In particular, fig. 5(c) shows how the determinant of the Jacobian calculated along the limit cycle orbit change for $\epsilon = 0.06$ (blue line) and $\epsilon = 0.1$ (red line), respectively. For smaller ϵ, one may identify two particular points where the determinant of the Jacobian is the largest, *i.e.*, where the impact of external perturbation is felt the strongest. This implies that noise is most likely to drive the systems trajectory away from the limit cycle attractor around these two sections of the orbit, which should lie closest to the boundary to the stability basins of the stationary states. Such a physical picture is maintained for larger ϵ, but one should stress that the sensitivity of limit cycle attractor to external perturbation substantially increases along the entire orbit, cf. fig. 5(c). In other words, faster adaptivity enhances the impact of noise, contributing to a more pronounced ISR effect. This point is addressed from another perspective in the next section.

We also examine the robustness of ISR to different modalities of the plasticity rule specified by β. Figure 6 shows how the average oscillation frequency changes with β and D for fixed $\epsilon = 0.05$. The non-linear response to noise, conforming to a resonant effect with a minimum of oscillation frequency at an intermediate noise level, persists in a wide range of β, essentially interpolating between the Hebbian-like and the STDP-like adaptive dynamics.

Fast-slow analysis: role of plasticity in the resonant effect. – Though ISR is observed for intermediate ϵ, here we show that the fast-slow analysis may still be applied to demonstrate a peculiar feature of the mechanism behind the resonant effect. In particular, we find that the plasticity enhances the resonant effect by driving the fast flow dynamics toward the parameter domain where the stationary state is a focus rather than a node. It is well known that the response to noise in multi-timescale systems qualitatively depends on the character of stationary states. Indeed, by using the sample-paths approach and other advanced techniques, it has already been shown that such systems may exhibit fundamentally different scaling regimes with respect to noise variance and the scale-separation ratio [27,28]. Moreover, the resonant effects may typically be expected in the case in which quasi-stationary states are focuses [27], essentially because the local dynamics around the stationary state then involves an eigenfrequency.

Within the standard fast-slow analysis, one may either consider the layer problem, defined on the fast timescale, or the reduced problem, concerning the slow timescale [29]. For the layer problem, the fast flow dynamics $\varphi_1(t;\kappa_1,\kappa_2), \varphi_2(t;\kappa_1,\kappa_2)$ is obtained by treating the slow variables κ_1 and κ_2 as system parameters, whereas in the case of the reduced problem, determining the dynamics of the slow flow $(\kappa_1(t), \kappa_2(t))$ involves time-averaging over the stable regimes of the fast flow of the layer problem. The fast flow can in principle exhibit several attractors, which means that multiple stable sheets of the slow flow may emerge from the averaged dynamics on the different attractors of the fast flow. Our key point concerns the dynamics of the slow flow, which requires us to first classify the attractors of the fast flow.

The fast flow dynamics is given by

$$\begin{aligned} \dot{\varphi_1} &= I_0 - \sin\varphi_1 + \kappa_1 \sin(\varphi_2 - \varphi_1), \\ \dot{\varphi_2} &= I_0 - \sin\varphi_2 + \kappa_2 \sin(\varphi_1 - \varphi_2), \end{aligned} \tag{2}$$

where $\kappa_1, \kappa_2 \in [-1, 1]$ are considered as additional system parameters. One may formally obtain (2) by setting $\epsilon = 0$ in (1) with $D = 0$. We find that the fast flow is monostable for most of the (κ_1, κ_2) values, exhibiting either a stable equilibrium or a limit cycle attractor, see fig. 7(a). In general, the fast flow admits either two or four fixed points, and a more detailed physical picture, including the associated bifurcations, is presented in [21]. The stability region of the oscillatory regime, outlined by the red color, has been calculated by numerical continuation starting from a stable periodic solution. Bistability between a stable fixed point and a limit cycle is observed only in a small area near the main diagonal $\kappa_1 = \kappa_2$. Within the region featuring oscillatory regime, each periodic solution obtained for (κ_1, κ_2) above the main diagonal has a Z_2 symmetry-related counterpart below the diagonal. Typically, the periodic solutions emanate from SNIPER bifurcations, which make up two branches where either κ_1 or κ_2 are almost constant and close to zero.

Using the results from the analysis of the layer problem, our goal is to determine the vector fields corresponding to the stable sheets of the slow flow. We have numerically obtained the dynamics of the slow flow by a standard two-step approach [19,30]. First, for fixed values (κ_1, κ_2), we have determined the time-averaged dynamics of the fast flow (2), $\langle \varphi_2 - \varphi_1 \rangle_t = h(\kappa_1, \kappa_2)$, whereby the averaging $\langle \cdot \rangle_t$ is carried out over a sufficiently long time interval, having excluded the transient behavior. As already indicated, such an average depends on the attractor of the fast flow for the given (κ_1, κ_2). If the fast flow possesses

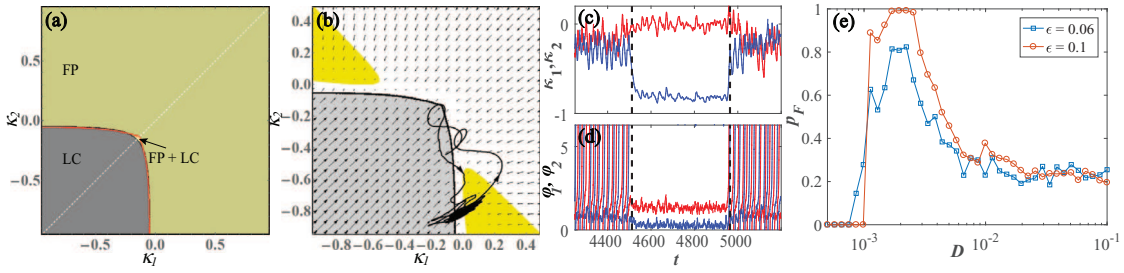

Fig. 7: (Color online) (a) Attractors of the fast flow (2) in terms of κ_1 and κ_2, now treated as free parameters. The fast flow is typically monostable, admitting either a stable fixed point (FP) or a stable limit cycle (LC), apart from a small region of bistability (FP+LC) around the main diagonal. (b) Vector field of the slow flow (3) determined by considering only the stable regimes of the fast flow for $\beta = 4.2, I_0 = 0.95$. Within the yellow-highlighted regions, the stable fixed point of the fast flow is a focus rather than the node. The displayed orbit $(\kappa_1(t), \kappa_2(t))$ corresponds to a switching episode from the oscillatory state to the quasi-stationary state and back (evolution direction indicated by arrows). Panels (c) and (d) show the time traces of phases and couplings during the switching episode. (e) Conditional probability $p_F(D)$ for $\epsilon = 0.06$ (blue squares) and $\epsilon = 0.1$ (red circles).

a stable fixed point, then $\langle \varphi_2 - \varphi_1 \rangle_t = \varphi_2^* - \varphi_1^*$, which corresponds to the slow critical manifold of the system. For (κ_1, κ_2) where the attractor of the fast flow is a periodic solution, $\langle \varphi_2 - \varphi_1 \rangle_t$ amounts to the time average over the period. Averaging over a periodic attractor of the fast flow is a standard approximation [30], quite natural when describing the influence of oscillations in the fast flow to the dynamics of the slow flow.

As the second step, the obtained time averages are substituted into the coupling dynamics

$$\begin{aligned} \dot{\kappa_1} &= \epsilon[-\kappa_1 + \sin(h(\kappa_1, \kappa_2) + \beta)], \\ \dot{\kappa_2} &= \epsilon[-\kappa_2 + \sin(-h(\kappa_1, \kappa_2) + \beta)]. \end{aligned} \tag{3}$$

The system (3) allows one to determine the vector fields on the stable sheets of the slow flow, which correspond to the attractors of the fast flow. In fig. 7(b), the vector fields associated to each of the attractors (fixed point or limit cycle) are presented within its respective (κ_1, κ_2) stability region. In the small region of the (κ_1, κ_2)-plane supporting coexisting stable solutions of the fast flow, the corresponding vector field of the slow flow is given on multiple overlapping sheets, since the value of the average $f(\kappa_1, \kappa_2)$ depends on the initial conditions.

Within the above framework, one is able to explain a subtle influence of adaptivity on the mechanism behind the ISR. To this end, in fig. 7(b) we have projected a typical example of the $(\kappa_1(t), \kappa_2(t))$ trajectory of the full system (1) corresponding to a switching episode between the metastable states associated to a limit cycle attractor and a stable equilibrium of the deterministic system, see the time traces in figs. 7(c), (d). One observes that for the oscillating regime, the coupling dynamics always remains close to the SNIPER bifurcation of the fast flow, cf. fig. 7(a), which makes the oscillations quite susceptible to noise. Recall that the fast flow is typically monostable. Thus, switching events in the full system are naturally associated to the fast flow undergoing the SNIPER bifurcation: either a direct one, leading from the oscillatory to the stationary regime, or the inverse one, unfolding in the opposite direction. For (κ_1, κ_2) values immediately after the SNIPER bifurcation toward the quiescent state, the stable equilibrium of the fast flow is a node. Nevertheless, for the noise levels where the effect of ISR is most pronounced, we find that the coupling dynamics guides the system into the region where the equilibrium is a stable focus rather than a node, see the yellow highlighted region in fig. 7(b). We have verified that this feature is a hallmark of the resonant effect by numerically calculating the conditional probability p_F that the events of crossing the SNIPER bifurcation are followed by the system's orbit visiting the (κ_1, κ_2) region where the stable equilibrium is a focus. The $p_F(D)$ dependences for two characteristic ϵ values at fixed $\beta = 4.2$ are plotted in fig. 7(e). One learns that $p_F(D)$ has a maximum for the resonant noise levels, where the corresponding curve $f(D)$ displays a minimum. In other words, the fact that the coupling dynamics drives the fast flow to the focus-associated regions of the (κ_1, κ_2)-plane results in trapping the phase variables for a longer time in the quasi-stationary (quiescent) state. Small noise below the resonant values is insufficient to drive the system to this region, whereas for too large a noise, the stochastic fluctuations completely take over, washing out the quasi-stationary regime. Note that for the faster adaptivity rate, the facilitatory role of coupling becomes more pronounced, as evinced by the fact that the curve $p_F(D)$ for $\epsilon = 0.1$ lies above the one for $\epsilon = 0.06$.

Discussion. – In the present paper, we have demonstrated a novel generic scenario for the onset of ISR, which involves an interplay between the local excitability feature and the adaptive dynamics of the couplings. For the example of two active rotators with coupling plasticity, we have shown that the spiking frequency corresponding to emergent oscillations varies non-monotonously with noise, displaying a minimum at a preferred noise level. Though the model *per se* is simplified, the underlying paradigm is relevant for combining the two core features of typical neuronal systems. The effect derives from the multi-timescale structure of the system, whereby the scale

separation between the local and the weight dynamics is tuned via adaptivity rate. Within a range of intermediate adaptivity rates, the deterministic dynamics of the full system exhibits multistability between the limit cycle attractors and the stable equilibria, each appearing in pairs due to the systems invariance to Z_2 symmetry. Applying the standard fast-slow analysis, we have shown that the resonant effect with noise is in fact plasticity-enhanced: plasticity promotes the impact of noise by guiding the fast flow toward the parameter domain where the stable equilibria become focuses instead of nodes. This mechanism increases the trapping efficiency by which the noise is able to deviate the systems trajectory from the metastable oscillatory states to the non-spiking regime. For faster adaptivity, the resonant effect is found to be more pronounced in a sense that the frequency dependence on noise shows deeper minima. Our scenario has proven to persist in a wide range of plasticity rules, interpolating between the cases analogous to Hebbian learning and STDP.

In earlier studies, observation of ISR has mostly been confined to Type-II neurons with intrinsic bistable dynamics, as in case of Hodgkin-Huxley or Morris-Lecar neurons near the subcritical Hopf bifurcation [3,6–9]. Even in case of networks, the macroscopic ISR effect has been linked to dynamical features of single units, only being modulated by the details of synaptic dynamics and the network topology [10]. In contrast to that, our results show that ISR may not rely on bistability of local dynamics, but may rather emerge due to the facilitatory role of coupling, here reflected in the interplay of multiscale dynamics and plasticity. Another distinction from most of the previous studies is that our scenario concerns Type-I units. For this class of systems, it is known that the dependence of the oscillating frequency of a single unit with noise is just monotonous [3,12], so that the resonant effect can only be observed in case of coupled units. So far, the latter case has been analyzed only once [5], but the underlying scenario is different from ours insofar as it involves static, rather than the adaptive couplings, and the effect *per se* is confined to a narrow region of the parameter space.

Quite recently, the onset of ISR has been reported for a single Fitzhugh-Nagumo oscillator [12], which is the first observation of the effect for Type-II neuron model in the vicinity of the supercritical Hopf bifurcation. Similar to the scenario we elaborated, ISR there also derives from the multiscale structure of the system. However, the actual mechanism behind the effect is associated to phase-sensitive (non-uniform) excitability of a limit cycle orbit conforming to relaxation oscillations [12]. These findings and the results here suggest that ISR may indeed provide a generic means of controlling and optimizing the firing rate in multi-timescale systems, which can be applied to neuronal activity, calcium signaling and other types of cell dynamics.

* * *

IF and IB would like to thank M. Wolfrum and S. Yanchuk for useful discussions. The work of VK on the third section was supported by the Russian Science Foundation, grant No. 16-42-01043. The work of VN on the fourth section was supported by the Russian Science Foundation, grant No. 14-12-01358.

REFERENCES

[1] Lindner B., Garcia-Ojalvo J., Neiman A. and Schimansky-Geier L., *Phys. Rep.*, **392** (2004) 321.
[2] McDonnell M. D. and Ward L. M., *Nat. Rev. Neurosci.*, **12** (2011) 415.
[3] Schmerl B. A. and McDonnell M. D., *Phys. Rev. E*, **88** (2013) 052722.
[4] Gammaitoni L., Hänggi P., Jung P. and Marchesoni F., *Rev. Mod. Phys.*, **70** (1998) 223.
[5] Gutkin B. S., Jost J. and Tuckwell H. C., *EPL*, **81** (2008) 20005.
[6] Tuckwell H. C., Jost J. and Gutkin B. S., *Phys. Rev. E*, **80** (2009) 031907.
[7] Uzuntarla M., Cressman J. R., Ozer M. and Barreto E., *Phys. Rev. E*, **88** (2013) 042712.
[8] Uzuntarla M., *Phys. Lett. A*, **377** (2013) 2585.
[9] Uzuntarla M., Torres J. J., So P., Ozer M. and Barreto E., *Phys. Rev. E*, **95** (2017) 012404.
[10] Uzuntarla M., Barreto E. and Torres J. J., *PLoS Comput. Biol.*, **13** (2017) e1005646.
[11] Buchin A., Rieubland S., Häusser M., Gutkin B. S. and Roth A., *PLoS Comput. Biol.*, **12** (2016) e1005000.
[12] Franović I., Omel'chenko O. E. and Wolfrum M., *Chaos*, **28** (2018) 071105.
[13] Hahn T. T. G., McFarland J. M., Berberich S., Sakmann B. and Mehta M. R., *Nat. Neurosci.*, **15** (2012) 1531.
[14] Franović I. and Klinshov V., *Chaos*, **28** (2018) 023111.
[15] Franović I. and Klinshov V., *EPL*, **116** (2016) 48002.
[16] Song S., Miller K. D. and Abbott L. F., *Nat. Neurosci.*, **3** (2000) 919.
[17] Froemke R. C. and Dan Y., *Nature*, **416** (2002) 433.
[18] Wang H.-X., Gerkin R. C., Nauen D. W. and Bi G.-Q., *Nat. Neurosci.*, **8** (2005) 187.
[19] Lücken L., Popovych O. V., Tass P. A. and Yanchuk S., *Phys. Rev. E*, **93** (2016) 032210.
[20] Kasatkin D. V. and Nekorkin V. I., *Radiophys. Quantum Electron.*, **58** (2016) 877.
[21] Bačić I., Yanchuk S., Wolfrum M. and Franović I., *Eur. Phys. J. ST*, **227** (2018) 1077.
[22] Kasatkin D., Yanchuk S., Schöll E. and Nekorkin V., *Phys. Rev. E*, **96** (2017) 062211.
[23] Destexhe A. and Rudolph-Lilith M., *Neuronal Noise* (Springer, New York) 2012.
[24] Maistrenko Y. L., Lysyansky B., Hauptmann C., Burylko O. and Tass P., *Phys. Rev. E*, **75** (2007) 066207.
[25] Aoki T. and Aoyagi T., *Phys. Rev. Lett.*, **102** (2009) 034101.
[26] Aoki T. and Aoyagi T., *Phys. Rev. E*, **84** (2011) 066109.
[27] Berglund N. and Gentz B., *Noise-Induced Phenomena in Slow-Fast Dynamical Systems* (Springer, Berlin) 2006.
[28] Laing C. and Lord G. J. (Editors), *Stochastic Methods in Neuroscience* (Oxford University Press, London) 2009.
[29] Kuehn C., *Multiple Time Scale Dynamics* (Springer International Publishing, Switzerland) 2015.
[30] Shilnikov A., *Int. J. Bifurcat. Chaos*, **18** (2008) 2141.